INTERNATIONAL JOURNAL OF AUTOMOTIVE AND MECHANICAL ENGINEERING
ISSN: 2229-8649 e-ISSN: 2180-1606
VOLUME 23, ISSUE 1, 2026, 13247 - 13262
DOI: https://doi.org/10.15282/ijame.23.1.2026.7.1005

RESEARCH ARTICLE

A 14 V battery-supercapacitor hybrid power supply for vehicle low-voltage systems: Reducing battery stress and enhancing dynamic response

Caihong Yan, Guoqing Ma, Guizhou Ren*

School of Electromechanical and Automotive Engineering, Yantai University, 264000 Yantai, China

Abstract – In response to the inherent limitations of single-battery low-voltage supply and the escalating demand for electrical equipment power in vehicles, the feasibility of replacing single-battery with battery/supercapacitor (SC) hybrid power supply (HPS) has been proposed and verified. This HPS directly connects a lithium-ion battery in parallel with the SC and combines a bidirectional DC-DC power converter to boost the voltage to the required level. It can drive the vehicle at low speeds and power electrical equipment. A MATLAB/Simulink model is constructed and simulated using the Federal Test Procedure-75 driving cycles. In addition, experiments are conducted to verify the HPS's boost characteristics. Furthermore, a case study is conducted to compare the proposed HPS with 14 V and 48 V single-battery systems under the China Light-duty Vehicle Test Cycle-Passenger Car operating condition. The results indicate that during frequent load fluctuations, the SC quickly responds to dynamic power and high-power demands, thereby significantly reducing battery stress. The proposed HPS demonstrates key advantages by enhancing dynamic response capability, reducing battery stress to extend lifespan, and improving energy efficiency. This study provides a new solution for the practical application of low-voltage power supply in vehicles.

Article History
Received : 12 July 2025
Revised : 28 November 2025
Accepted : 12 January 2026
Published : 10 March 2026

Keywords
Battery-supercapacitor
14 V hybrid power supply
Boost characteristics

1. Introduction

The increasing energy crisis and environmental pollution have prompted green and low-carbon vehicles to become the direction of development in the automotive industry [1–2]. Consequently, more stringent requirements have been set for vehicle performance indicators and energy utilization [3–4]. Therefore, the development of efficient power systems for vehicles has emerged as an urgent priority [5]. Electric energy storage technology has marked a milestone in transforming vehicle power systems and has become the driving force of technological evolution in this field [6]. The current mainstream technologies primarily include batteries, superconducting magnetic, flywheels, and supercapacitors (SCs). Superconducting magnetic exhibits high efficiency, rapid response, long lifespan, and environmental friendliness. However, due to high costs and the need for low-temperature maintenance, its application for instantaneous power compensation is currently limited to laboratories or high-end concept vehicles. Flywheels have been used in bus regenerative braking systems due to their high power density and long cycle life. However, mechanical safety risks and volume limitations make it better suited to commercial vehicles. Batteries are the most popular energy storage technology, capable of storing large amounts of electrical energy while providing a stable energy output. The main battery types include nickel-metal hydride, solid-state, sodium-ion, and lithium-ion (LIB). Notably, LIBs demonstrate superior overall performance in terms of energy density, power characteristics, self-discharge rate, and cost efficiency, making them the predominant choice for new energy vehicles (NEVs) [7]. As an emerging energy storage device, SC exhibits excellent fast charging/discharging capabilities, a million-cycle lifespan, and low-temperature resistance. It can deliver high-power, instantaneous output during transient demand and is widely used in regenerative braking systems for hybrid electric vehicles. However, its relatively low energy density limits the storage capacity [8]. It is worth noting that LIB and SC exhibit significant complementary characteristics, with LIB steadily supplying energy at high energy density. At the same time, SC can meet instantaneous power demands through high power density and millisecond-level charging/discharging speed. The combination of the two technologies enables simultaneous delivery of stable energy output and rapid power response under complex driving conditions [9]. This configuration offloads high-frequency charging/discharging tasks to SC, thereby extending battery life and optimizing energy efficiency [10–11]. The hybrid power supply (HPS) can maintain stable operation over a broad temperature range of –40 °C to 85 °C, achieving a more competitive overall cost by reducing battery usage and realizing the technological synergy effect of "1+1 > 2".

The application of HPS integrating battery and SC in vehicles has achieved dual improvements in power performance and energy efficiency through functional complementarity and technological synergy. As the core component of the start-stop system, HPS automatically shuts down the engine under idle conditions and relies on SC for power to keep electrical equipment operational. This design not only reduces fuel consumption at idle but also extends battery life by leveraging SC's fast-discharging capability. When the driver steps on the accelerator, the battery and the SC work together to start the engine in milliseconds. Additionally, as a low-voltage power supply, HPS can instantly deliver high power via SC when the battery voltage is insufficient, preventing vehicle stalling and enhancing system reliability. In terms of auxiliary power and propulsion support, HPS provides instantaneous high power via SC to compensate for inadequate battery output, ensuring reliable starting and smooth vehicle acceleration.

HPS enhances vehicle dynamic performance through an energy-buffering mechanism. For example, during braking, SC recovers braking energy and converts it into electrical energy for storage. During acceleration, SC releases the stored

*CORRESPONDING AUTHOR | G. Z. Ren | ✉ lucky_my2008@163.com
© 2026 The Author(s). Published by Universiti Malaysia Pahang Al-Sultan Abdullah Press. This is an open access article under the CC BY-NC 4.0 International license

electrical energy. In addition, HPS achieves efficient energy utilization through allocation strategies, such as prioritizing battery power during low-load conditions, while SC actively supplies power to reduce high-current stress on the battery during high-load conditions. Moreover, SC can maintain stable operation over a wide temperature range of 85 °C to –40 °C, overcoming the limitations of battery performance at low temperatures. Therefore, HPS can improve the low-temperature start-up performance of vehicles under extreme conditions. As mentioned above, HPS has achieved comprehensive upgrades in start-stop control, power assistance, energy recovery, and efficiency optimization through complementary functions, becoming an essential direction for the development of vehicle power technology. Future research can focus on developing energy management and fault-diagnosis methods based on artificial intelligence (AI) to achieve intelligent HPS. In addition, the feasibility of HPS in multi-scenario applications can also be explored, such as low-voltage power supply and vehicle-to-grid interaction modes. These breakthroughs will drive the transformation of HPS from a single power system to an intelligent energy hub, providing key technological support for the sustainable development of the vehicle industry.

At present, the battery/SC HPS has established a mature paradigm, characterized by passive, semi-active, and fully active configurations, and the overall architecture is stabilizing. The passive structure is simple, highly reliable, and responsive, but it fails to leverage the advantages of both components fully. The semi-active structure improves energy management flexibility and parameter matching by introducing a power converter at a moderate cost. However, energy management is limited, and control strategies are complex. The fully-active structure enables highly flexible energy management, fully leverages component advantages, and offers strong adaptability. However, it suffers from a complex structure, high costs, challenging control, and potential efficiency losses [12]. Furthermore, in specific application scenarios, such as electric vehicle (EV) and energy storage, where multiple predetermined constraints (e.g., power, energy, volume, and cost) must be considered, the configuration space for the combination of key parameters (e.g., capacity and voltage) of two power sources is relatively limited. This makes it challenging to achieve significant further optimization at the system configuration level. Due to the optimization bottleneck in the topology structure mentioned above, the current focus in academia and industry has shifted toward the refined design and dynamic regulation of energy management strategies. Research driven by intelligent optimization algorithms aims to improve decision performance through innovative biomimetic algorithms. For example, Li et al. [13] introduced an energy management optimization strategy for HPS combining the Hybrid Chimpanzee Optimization Algorithm with the Levy Flight Algorithm. Verification results demonstrated that this approach enhances overall EV performance and that, compared with a traditional single-battery system, the lifespan of the battery in HPS has increased by 19%. Kannan et al. [14] proposed a strategy that combines jellyfish search (JS) with the gradient-boosting decision tree algorithm. Alkawak et al. [15] studied an integrated framework combining quantum neural networks with the nanocloth beetle optimization algorithm; the effectiveness of this optimization strategy has been empirically verified. The model predictive control (MPC)-based method focuses on dynamic adaptability to working conditions. For example, Chen et al. [16] and Nguyen et al. [17] studied energy control strategies of HPS using MPC. The implementation results for online prediction show that this strategy can alleviate pressure on the battery, reducing energy consumption by 15.3% compared to the fuzzy-logic-based strategy. It can be seen that it achieves dual benefits of reducing energy consumption and mitigating battery degradation under dynamic load conditions.

Multi-algorithm comparison and collaborative optimization solutions are dedicated to technological integration and innovation. For example, Ren et al. [18] used the grey wolf algorithm and a genetic algorithm to construct an energy-efficiency model to optimize the power allocation strategy. The comparison results showed that the optimization algorithm-based methods achieved higher efficiency from 87% to 91%. In addition, the average efficiency of the optimization strategy under the New European Driving Cycle operating condition exceeded 85%, further confirming that the optimization strategy improves energy utilization efficiency. Robayo et al. [19] constructed a power allocation framework based on predictive theory to optimize the energy utilization efficiency of SC. The results showed that it effectively improved energy conversion efficiency and reduced the battery's current stress during transient events, such as acceleration and braking. Some comprehensive evaluation studies have analyzed the technical benefits of HPS from a macro perspective. For example, Ren et al. [20] developed an energy-efficiency optimization framework that accounts for energy consumption indicators. Control strategies based on three optimization algorithms have been established, with energy consumption rate as the objective. The results showed that the maximum average energy efficiency and the minimum average energy consumption rate reach 87.5% and 0.146 kWh/km, respectively. This study indicates that combining HPS with optimized control strategies can significantly improve economic benefits. Lin et al. [12] conducted an in-depth analysis of power allocation methods for HPS, critically evaluating the technical advantages and implementation limitations of various techniques. This review provides valuable resources for related research work. Ren et al. [21] conducted a thorough analysis of the energy-saving potential of HPS in EV applications, confirming that significant economic and environmental benefits can be achieved through advanced power management strategies.

Compared to restructuring established hardware, optimization strategies are considered a more promising and effective path. Practice has shown that through strategy optimization, the system's comprehensive performance can be effectively improved on existing hardware platforms, including enhanced dynamic response, smoother power fluctuations, extended battery life, and ultimately improved reliability and economy of the HPS. Overall, existing research provides hierarchical theoretical support for the application of HPS across different scenarios, including fundamental algorithm innovation, multi-algorithm collaboration, dynamic control frameworks, and benefit evaluation.

The current research results have demonstrated the superiority of the battery/SC HPS, which provides a solid theoretical basis for its application as the primary power supply for EVs. However, it should be noted that the vast majority of

research has focused on HPS as a high-voltage power supply for EVs. Researchers have proposed complex topological structures and advanced optimization theories for high-voltage HPS used in EVs, aiming to achieve performance breakthroughs. In contrast, research on low-voltage HPS for vehicles remains scarce, and this field has not been fully explored. To address this research gap, this study focuses on the feasibility of replacing conventional single-battery low-voltage power supply in vehicles with the battery/SC HPS. As is well known, there are fundamental differences between low-voltage power supplies and high-voltage power supplies in terms of functionality, technical characteristics, efficiency, and safety. Due to its voltage level and power capacity, the high-voltage power supply can withstand the additional overhead caused by complex topologies and control algorithms. In contrast, the low-voltage power supply has poor tolerance. If a complex topology is used in a low-voltage power supply, it will not only increase energy losses and reduce efficiency but also increase the complexity of the control system, thereby affecting operational stability. Although optimization algorithms can partially improve performance, they also impose stricter hardware requirements on control systems, which can increase development costs and create technical barriers.

Therefore, based on a comprehensive analysis of the operation and practical requirements of low-voltage power supplies, this study adopts a conventional topology, in which the battery and the SC are directly paralleled and equipped with a bidirectional DC-DC power converter (BDPC). This approach combines structural simplicity, control convenience, and cost-effectiveness while maintaining fundamental system performance, thus proving its suitability for practical applications of low-voltage power supplies in vehicles. It is worth emphasizing that this study chooses the 14 V voltage platform as the research object. Firstly, as the mainstream low-voltage architecture used in vehicles, the 14 V platform has significant advantages in safety, maturity, and cost-effectiveness. In addition, it also provides a crucial technical validation foundation for transitioning to the highly anticipated 48 V power supply. The proposed solution eliminates the need to rebuild the electrical architecture, is fully compatible with existing components, and achieves dynamic voltage regulation through BDPC. Furthermore, the voltage can be increased to 48 V, seamlessly adapting to the 48 V electrical system. This technological approach not only retains the maturity advantage of the 14 V system but also provides technical reserves for modular upgrades of multi-voltage architectures. In addition, the current 14 V low-voltage power supply primarily uses a lead-acid battery, although its performance limitations have not received sufficient attention. Lead-acid batteries have obvious drawbacks, such as low energy efficiency due to heat loss and electrochemical polarization, standby current that can lead to power loss, and a limited energy density that can hinder support for high-power devices. In addition, there is a power response delay, and a significant increase in internal resistance at –20 °C will significantly reduce the cold start capability. LIBs are substantially better than lead-acid batteries in terms of cycle life, energy density, and low-temperature performance. Although the initial cost is 2–3 times that of a lead-acid battery, the lifecycle cost is lower, and a lightweight design also helps reduce energy consumption. Therefore, from both technical and economic perspectives, LIBs have excellent feasibility for replacing lead-acid batteries. However, research on HPS configurations combining LIB and SC as both a low-voltage power supply and auxiliary power unit in vehicles remains limited. Addressing this gap, this article proposes a LIB/SC HPS as an efficient, reliable, and flexible power solution for vehicles, an alternative to traditional low-voltage power supplies. This HPS not only supplies power to 14 V electrical equipment but also achieves voltage boosting for higher loads through the integration of a BDPC, thereby meeting the flexible needs of multi-mode power transmission. To verify the performance, a detailed HPS model is developed in MATLAB/Simulink and simulated under the Federal Test Program-75 (FTP-75) driving cycles. The FTP-75 is a standard test program and simulates urban road conditions, including cold starts, stable driving, and hot soaks, providing reliable data for HPS evaluation. Furthermore, an experimental platform is constructed to test the boost characteristics, energy efficiency, and stability of the HPS by simulating dynamic step-load changes. Finally, a case study is conducted under the China Light-duty Vehicle Test Cycle—Passenger Car (CLTC-P) operating condition, using 14 V and 48 V single-battery systems as comparison benchmarks with the proposed HPS.

2. Materials and Methods

2.1 Operating Principle of the HPS

The HPS configuration used in this study is shown in Figure 1. Under dynamic load conditions, due to its inherent low internal resistance, the SC can quickly respond to current fluctuations, while the battery maintains a stable baseline current supply. This complementary characteristic enables the HPS to simultaneously meet steady-state and transient power demands under variable operating conditions. Based on the vehicle's power demand, the HPS can operate in multiple modes. For example, 1) High power mode. By boosting the voltage through the BDPC to supply the load, the battery can provide stable power, while the SC can meet dynamic power requirements. 2) Energy feedback mode. The SC captures the majority of regenerative energy, thereby alleviating the stress on the battery. 3) Low power mode. The SC operates independently to provide electricity. Although the parallel structure limits the flexible adjustment of the voltage of two power sources, which may restrict capacity utilization and load-balancing efficiency, this configuration offers a significant advantage: a simple structure. The HPS architecture effectively leverages the SC's efficient, fast charging/discharging capabilities. When it is necessary to enhance power output, such as during vehicle start-up and acceleration, the HPS will quickly release stored energy to provide instantaneous or short-term high-power support. This configuration improves power response speed and performance, and reduces battery pressure by avoiding high-power discharge requirements. This study utilizes the built-in LIB model in MATLAB (as shown in Figure 2) [22], where $Sel(s)$ represents the battery mode and $Exp(s)$ denotes the exponential zone dynamics. E_{Batt} and E_{Batt} are the nonlinear voltage and terminal voltage, respectively. i_{Batt} and R_{Batt} represent the current and internal resistance, respectively. E_0 is the constant voltage, K is the polarization constant/resistance, Q is the maximum battery capacity, and A and B are the

exponential voltage and exponential capacity, respectively. i^* is the low-frequency current dynamics, and i is the battery current; it is the extracted capacity.

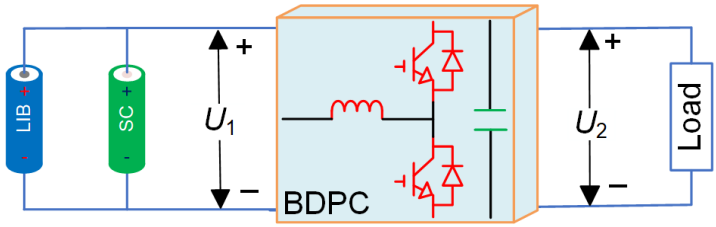

Figure 1. The HPS configuration

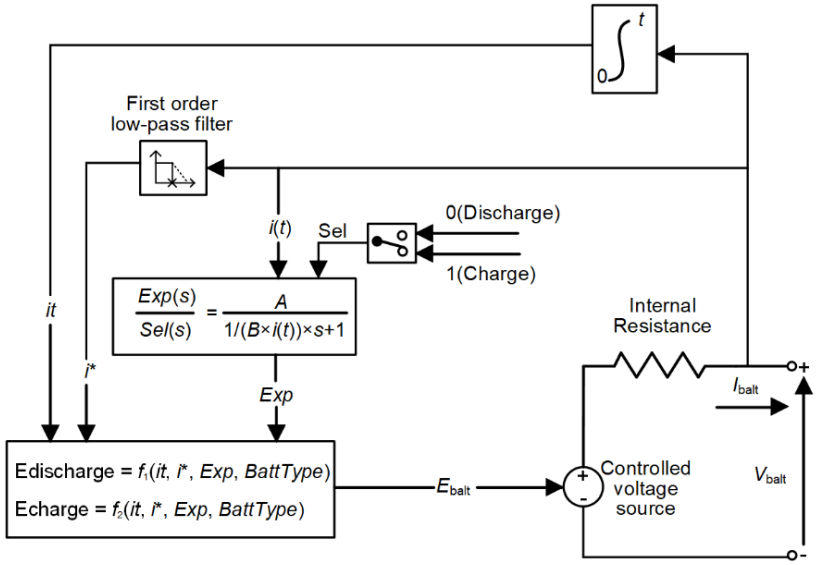

Figure 2. The LIB model

It can be seen that it is a dynamic modeling framework based on equivalent circuits and state equations. The input current is processed by a first-order low-pass filter, which is then used to determine the battery's charging and discharging states. Internal losses are simulated using a variable internal resistance, and the open-circuit voltage is calculated by combining state equations that account for the battery type, aging factor, smoothed current, and actual current. The dynamic characteristics of charging/discharging are accurately simulated by outputting the terminal voltage via a controlled voltage source. This model is constructed based on general experimental data from typical batteries and provides a specific reference value.

The discharge model ($i^* > 0$) can be described as follows:

$$f_1(it, i^*, i) = E_0 - K \times \frac{Q}{Q - it} \times i^* - K \times \frac{Q}{Q - it} \times it + A \times \exp(-B \times it) \quad (1)$$

The charge model ($i^* < 0$) can be described as follows:

$$f_2(it, i^*, i) = E_0 - K \times \frac{Q}{it + 0.1 \times Q} \times i^* - K \times \frac{Q}{Q - it} \times it + A \times \exp(-B \times it) \quad (2)$$

$$V_{\text{batt}} = E_{\text{batt}} - i_{\text{batt}} \times R_{\text{batt}} \quad (3)$$

Additionally, since energy conversion and storage in the SC primarily rely on physical processes during charging/discharging cycles, this study adopts a simplified equivalent circuit model comprising an internal resistance and capacitance (as shown in Figure 3). This model sufficiently captures the essential dynamic characteristics of the SC, thereby fully meeting the requirements for both theoretical analysis and experimental validation in this research.

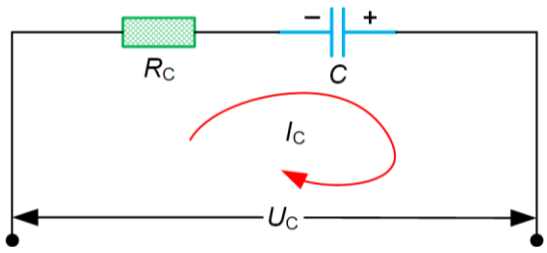

Figure 3. The SC model

The SC model adheres to:

$$\Delta U = \frac{I_C \times t}{C} \tag{4}$$

where I_C, C, and ΔU represent the SC current, capacity, and voltage change, respectively, and t is the time.
A non-isolated half-bridge bidirectional power converter is employed in the HPS to regulate power flow via power-switch modulation. When the HPS operates in boost mode for energy output, if V2 is conductive (VD2 is non-conductive), and V1 is non-conductive (VD1 is non-conductive), then the inductor (L) is charged. When V2 switches to a non-conductive state (with VD2 also non-conductive), and V1 remains non-conductive, the current commutates through VD1, causing the inductor (L) to discharge. The equivalent circuit is shown in Figure 4, which satisfies the following relationship:

$$U_2 = U_1 \times \frac{1}{1 - D_{V2}} \tag{5}$$

$$I_2 = I_1 \times (1 - D_{V2}) \tag{6}$$

where U_1 and U_2 denote the input and output terminal voltages, I_1 and I_2 represent the input and output currents, and D_{V2} is the duty cycle of power-switch V2.

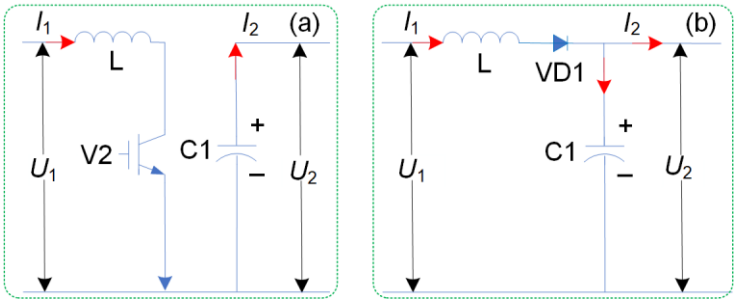

Figure 4. The equivalent circuit for boosting

During HPS buck-mode operation, power flow is controlled via power-switch modulation. When V1 is conductive (with VD1 blocked) and V2 and VD2 are blocked, the system enters the charging phase, during which the load energy and capacitor (C1) jointly supply power to the HPS. When V1 is blocked (with VD1 still blocked), the operation mode switches to capacitor charging because the load energy is transferred to charge C1. The equivalent circuit configuration (Figure 5) establishes the following relationship:

$$U_1 = U_2 \times D_{V1} \tag{7}$$

$$I_2 = I_1 \times D_{V1} \tag{8}$$

where D_{V1} is the duty cycle of the power-switch V1.

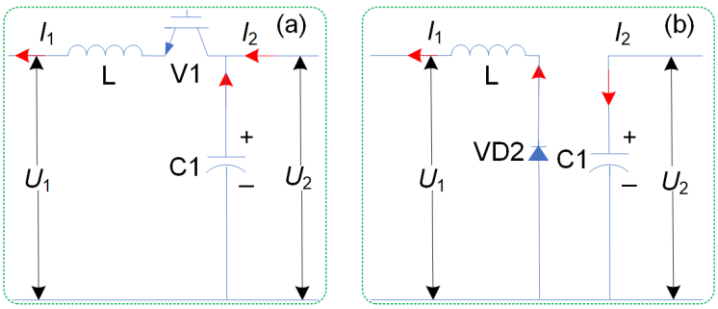

Figure 5. The equivalent circuit for voltage reduction

The power converter efficiency can be expressed as:

$$\varphi = \frac{I_{\text{out}} V_{\text{out}}}{I_{\text{in}} V_{\text{in}}} \times 100\% \tag{9}$$

where V_{out} and V_{in} denote the output and input voltages, while I_{out} and I_{in} represent the output and input currents, respectively.

Permanent magnet DC motors have found extensive applications in NEVs owing to their superior high-speed performance and substantial electromagnetic torque, as well as the proportional relationships between electromagnetic torque and current and between induced electromotive force (EMF) and speed. In this study, the load characteristics of the auxiliary power supply are simulated using a permanent-magnet DC motor, and the dynamic performance of the HPS is verified under the FTP-75 driving cycle. The simplified equivalent model (Figure 6) establishes the following voltage balance equation:

$$U_{\text{m}} = L_{\text{m}} \frac{\text{dI}_{\text{m}}}{\text{dt}} + r_{\text{m}} I_{\text{m}} + e \tag{10}$$

$$e = L_{\text{m}} \frac{\text{d}I_{\text{m}}}{\text{dt}} + r_{\text{m}} I_{\text{m}} + I_{\text{m}} R \tag{11}$$

where U_{m} denotes the terminal voltage, L_{m}, I_{m}, and r_{m} are the armature inductance, current, and resistance, respectively, e is the induced EMF, and R is the equivalent load.

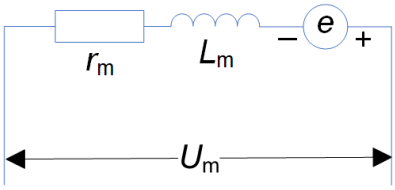

Figure 6. An equivalent model of the motor

2.2 Power Demand Under FTP-75 Driving Cycles

The FTP-75 driving cycles evaluate emissions and fuel efficiency for light-duty vehicles, comprising three phases totaling 1,875 seconds:

- Cold start transient phase: simulates vehicle startup from rest in 20–30 °C ambient conditions, lasting 505 seconds.
- Steady-state phase: during the 505th to 1370th seconds, the engine runs under stable conditions while the vehicle maintains the prescribed speed/acceleration profiles to evaluate steady-state emissions and fuel consumption.
- Hot start transient phase: starting from the 1370th second and lasting for 505 seconds, simulates the emission control when the engine restarts after a short period of vehicle parking.

The FTP-75 driving cycle replicates urban driving conditions, including frequent stop-and-go and temperature variations. The vehicle propulsion force during operation satisfies the following equation:

$$F_{\text{t}} = \text{mgsin}\alpha + \delta \text{ma} + \frac{C_{\text{D}} \text{Av}^2}{21.15} + \text{mgfcos}\alpha \tag{12}$$

where F_{t} is the vehicle propulsion force, m is the vehicle mass at maximum load, g is the gravitational acceleration, α is the road gradient, δ is the rotational mass conversion factor, C_{D} and f are the air resistance coefficient and the rolling resistance coefficient, respectively. A is the vehicle's frontal area, v is the speed, and a is the acceleration.

The vehicle power under driving conditions can be expressed as:

$$P(t) = \frac{v}{3600 \eta_{\text{T}}} \left(\text{mgsin}\alpha + \text{mgfcos}\alpha + \frac{C_{\text{D}} \text{Av}^2}{21.15} + \delta \text{ma}\right) \tag{13}$$

where η_{T} represents the transmission efficiency.

For the convenience of performance analysis of the HPS under the FTP-75 driving cycles, the steady-state phase (509–1370 s) and hot-start transient phase (1370–1500 s) are selected for simulation. Vehicle speed is halved, and the time axis is scaled by a factor of two. A power calculation model has been established utilizing MATLAB/Simulink as the development platform, as depicted in Figure 7. The simulated vehicle speed and required power profiles are presented in Figure 8. The scaled vehicle speed remains below 30 km/h, the maximum power is below 5 kW, and the load demand remains within the HPS's working range.

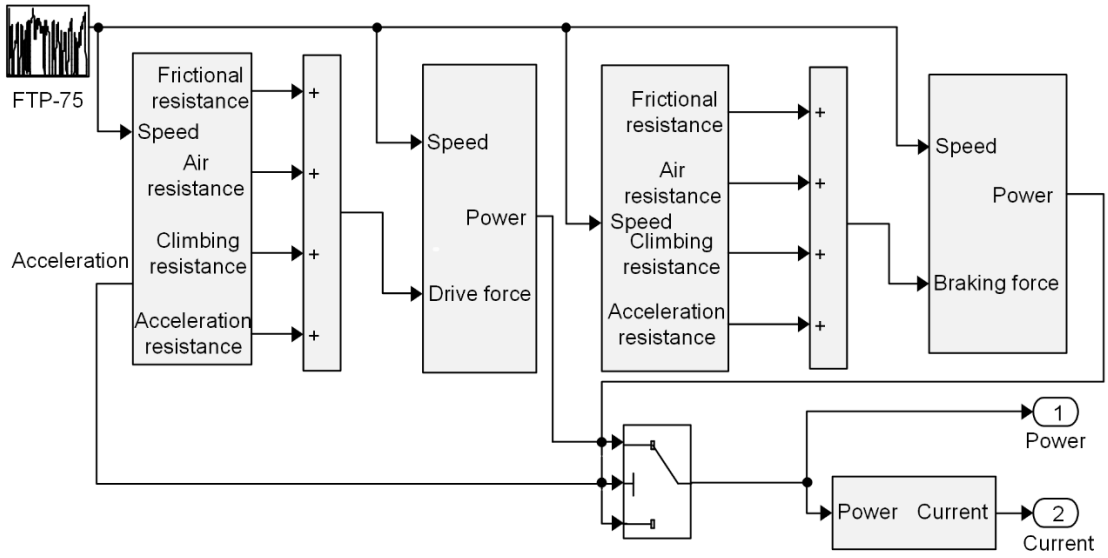

Figure 7. Power calculation model

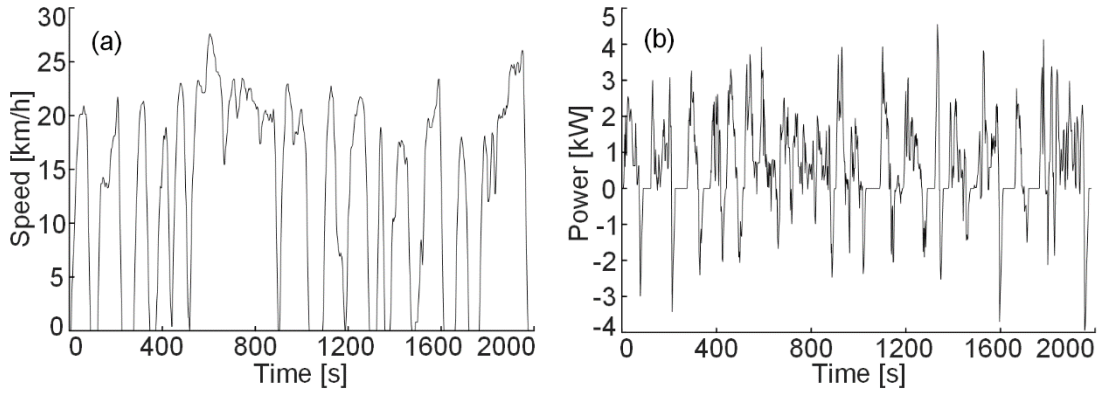

Figure 8. The FTP-75 operating condition: (a) vehicle speed, (b) required power below 5 kW

2.3 Simulation Model of the HPS

The simulation model of the HPS as depicted in Figure 9 comprises the LIB (initial voltage of 14 V, operating range of 10–14.6 V, capacity of 6.5 Ah, internal resistance of 20 mΩ, initial state of charge (SOC) of 0.8) and the SC (initial voltage of 14 V, operating range of 8.1–17.1 V, capacitance of 200 F, internal resistance of 3 mΩ, initial state of charge of 0.6), along with a BDPC, bridge-type inverter, motor, and proportional integral derivative (PID) controllers. The PID controllers regulate HPS current and Bus voltage to track reference trajectories, as shown in Figure 10.

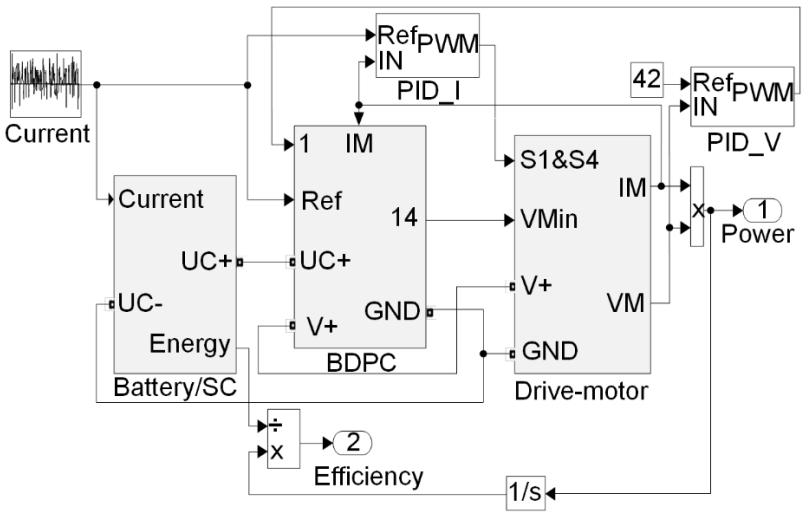

Figure 9. The HPS model

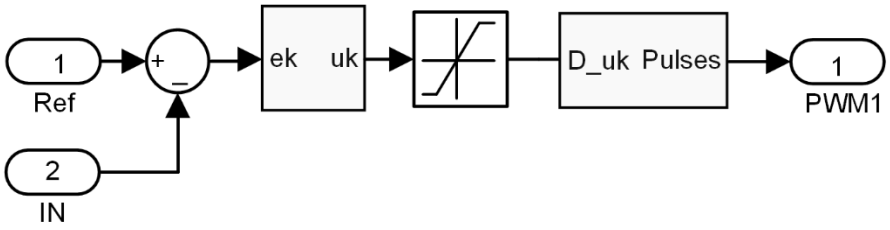

Figure 10. PID controller model

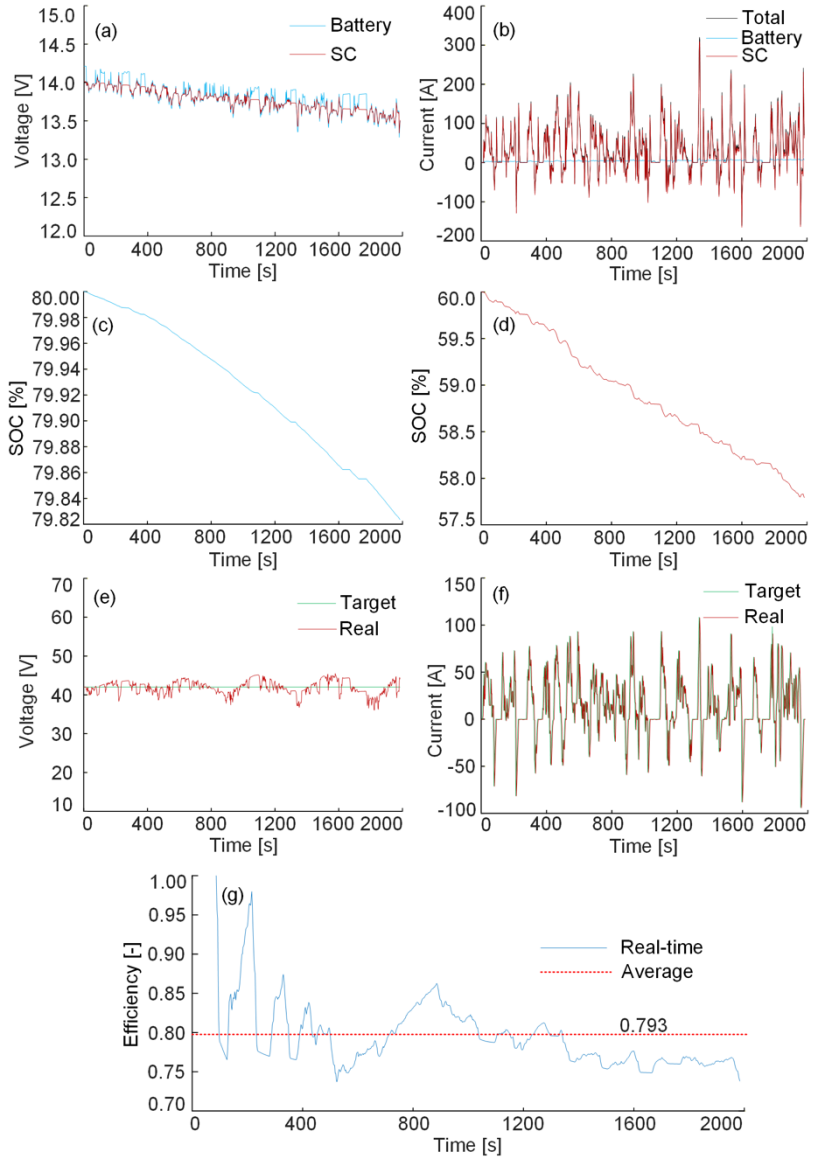

Figure 11. Simulation results under the FTP-75 operating condition: (a) HPS voltage, (b) HPS current, (c) battery SOC, (d) SC SOC, (e) Bus voltage, (f) load current, (g) efficiency

3. Results and Discussion

3.1 Simulation Under The FTP-75 Driving Cycles

As shown in Figure 11(a), both the battery voltage and SC voltage are maintained around 14 V. The HPS current profile in Figure 11(b) shows that dynamic current demand is primarily met by the SC, with a peak current of 309.97 A, while the battery provides a relatively stable current, with a maximum of only 19.21 A. The results clearly show that throughout the driving cycle, the SC provides the majority of the required current, with its current output significantly exceeding that of the battery. This configuration mitigates high-current stress on the battery, extending its operational lifespan. As shown in Figure 11(c) and Figure 11(d), the battery's SOC gradually decreased from 80% to about 79.82% while maintaining a relatively stable discharge rate. The SOC of the SC decreased from 60% to approximately 57.7%, with slight fluctuations observed in its discharge curve. This indicates that as a power-type component, the SC primarily handles dynamically

fluctuating power requirements, while the battery serves as an energy-type component supplying relatively stable, low-level power. The Bus voltage is set to 42 V. As shown in Figure 11(e), the PID controller effectively regulates the actual Bus voltage, maintaining minimal fluctuations around an average of 41.88 V. This demonstrates the HPS's ability to maintain stable voltage output under dynamic load conditions. The load current calculated based on the operating condition is used as the current target value, and a PID controller adjusts the actual load current. As shown in Figure 11(f), the actual current closely tracks the target value, and overshoot can be ignored. As shown in Figure 11(g), the HPS achieves an average efficiency of 79.3%, though the frequent acceleration/deceleration events characteristic of the FTP-75 driving cycles influence this efficiency. These dynamic conditions necessitate frequent energy conversions, contributing to increased energy losses. Nevertheless, the total energy loss remains relatively low, which is critical for sustaining efficient vehicle powertrain operation and enhancing overall energy utilization efficiency. From the results, it can be seen that the HPS effectively combines the inherent advantages of both power sources while mitigating their respective shortcomings through the collaborative operation of the battery and the SC. This configuration reduces the current stress on the battery, maintains a stable output voltage under complex driving conditions, and efficiently tracks the load current target, thereby demonstrating its feasibility in practical applications.

3.2 Testing based on variable load conditions

To verify the HPS's output stability and dynamic responsiveness under variable load conditions, a 14 V battery/SC HPS experimental platform is constructed in the laboratory, as shown in Figure 12. The main hardware of the experimental system is shown in Table 1. Voltage/current sensors are used to collect the HPS voltage, Bus voltage, HPS current, and load current. Adjustable power resistors are used as dynamic loads. A programmable DC power supply provides power to electrical components. The program code is written in the CCS 3.3 compilation environment, including setting initial values for the control objectives of bus voltage and load current, implementing a proportional-integral-derivative (PID) algorithm to achieve precise tracking of control targets, and writing programs for sensor signal conversion and pulse-width modulation (PWM) signal output. The program code is downloaded to the DSP control unit through the simulator to complete the implementation of control logic. In the experiment, the DSP control unit receives real-time voltage and current signals from sensors, dynamically adjusts the PWM signal duty cycle using a PID algorithm, and then controls the IGBT conduction and turn-off to track the target voltage and load current. The 8-channel oscilloscope is used to synchronously observe and record the waveform data for each channel, storing them in the oscilloscope's built-in storage unit. The Bus voltage is set to 24 V, and the dynamic load current is configured as follows: 10 A in the 0–2 seconds, 4 A in the 2–6 seconds, 6 A in the 6–7 seconds, and 8 A in the 7–10 seconds. The test results are presented in Figure 13.

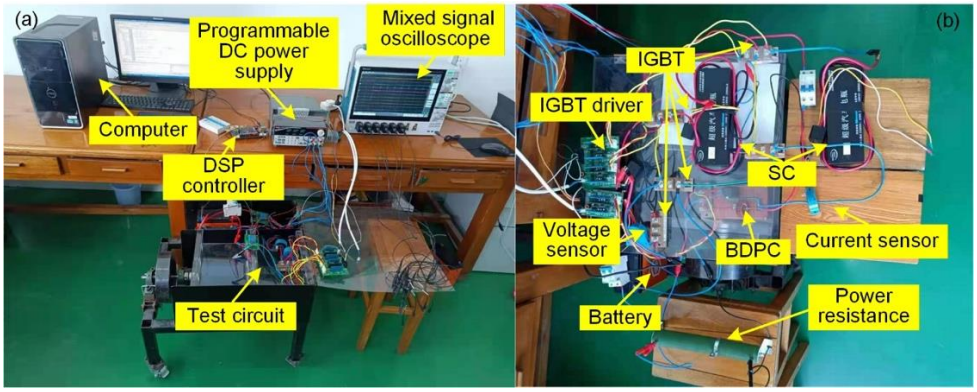

Figure 12. Experimental system: (a) platform, (b) test circuit

Table 1. The main hardware of the experimental system

Name	Model and specifications
Oscilloscope	8-channel mixed signal oscilloscope
DC power supply	2231A-30-3/3-channel 30 V/3 A
DSP control unit	TMS320F2812
Power sources	SC/14 V/58 F、LIB/14 V/9.6 A·h
IGBT and its driver	2MBI100VA-060-50/TX-DA962
Inductor of BDPC	330 μH/30 A
Electrolytic capacitor of BDPC	4700 μF/50 V
Adjustable power resistor	5 Ω/500 W, 10 Ω/300 W, 20 Ω/300 W, 50 Ω/100 W, 100 Ω/100 W
Hall voltage sensor	CHV-25P/±50V/0-75 V
Hall current sensor	CHF-25F/±25A/0-50 A

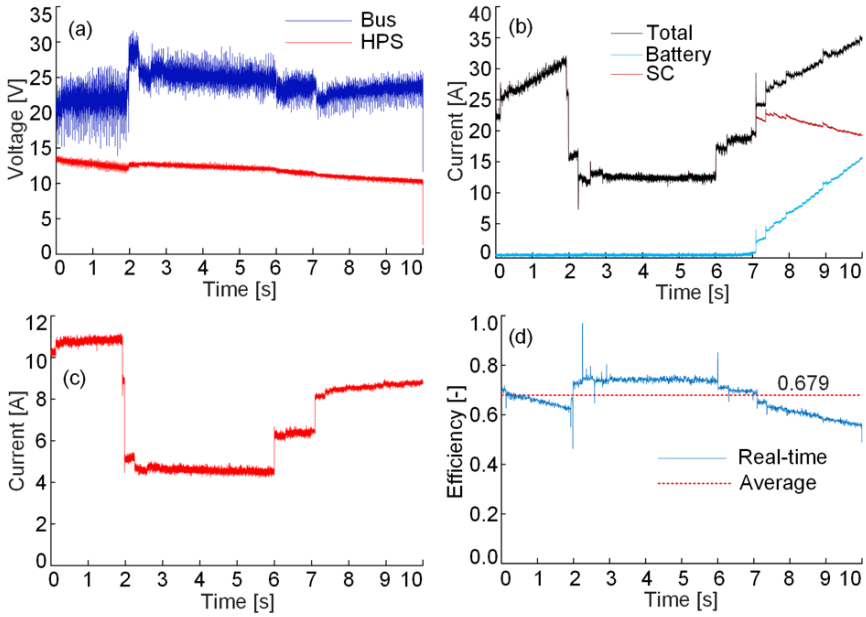

Figure 13. Experimental results (Bus voltage of 24 V): (a) HPS voltage and Bus voltage, (b) HPS current, (c) load current, (d) efficiency

As shown in Figure 13, during the 0–2 second interval (representing vehicle startup or instantaneous acceleration), a high-power demand (10 A load current) occurs, requiring significant current from the HPS. The SC independently meets the load power or motor torque requirements during this phase. After 2 seconds, the load current decreases to 4 A, with the SC providing all required power while the battery remains inactive (0 A output). During the 6–10 second phase (representing vehicle acceleration), the HPS must deliver increased power as the load current rises from 6 A to 8 A. The HPS current varies between 10 and 35 A, while the SC consistently supplies peak dynamic currents. This demonstrates effective utilization of the capabilities of peak-shaving and valley-filling of the SC, which significantly reduces battery stress by handling most transient power demands.

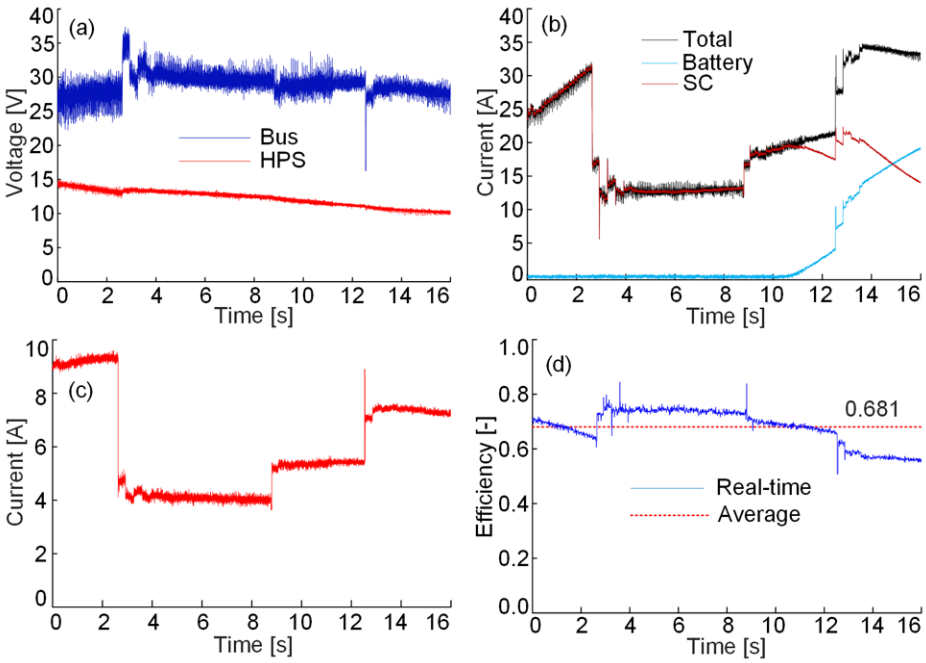

Figure 14. Experimental result (Bus voltage of 30 V); (a) voltages of HPS and Bus, (b) HPS current, (c) load current, (d) efficiency

The Bus voltage is set to 30 V, with the dynamic load current varying from 9 A to 4 A, then to 5 A, and finally to 7 A over a 16-second interval. As shown in Figure 14, the actual Bus voltage remains regulated near the 30 V target value throughout the discharge process, exhibiting minor fluctuations corresponding to load current changes. The HPS voltage gradually decreases from its initial value of 14 V. During the 0–2.5 second interval (e.g., startup or instantaneous vehicle

acceleration), the SC promptly responds to high-load current demands while the battery remains inactive. When the load current decreases to 4 A, the SC alone meets the demand. During the 9–16 second phase (representing the vehicle's acceleration), the battery and the SC collaborate to provide power. As the SC's energy depletes, its discharge current progressively decreases, while the battery's discharge current increases correspondingly. The current of the SC tracks the load current within 10–35 A, with the battery contributing a relatively small, stable proportion of current. This configuration effectively minimizes high-current stress on the battery. On the whole, the SC demonstrates rapid response to dynamic load variations, delivering instantaneous high current while maintaining relatively stable power output. Conversely, the battery primarily provides base-level, stable energy, avoiding high-current discharge and minimizing current fluctuations. Therefore, the 14 V low-voltage HPS effectively adapts to the complex driving conditions and improves power performance and energy efficiency through flexible power management. It should be noted that although the current tests have verified the dynamic response and voltage stability of the HPS under variable loads, the experimental setup has certain limitations. The experimental period only covers brief steady-state and transient processes, focusing on the instantaneous peak-shaving capability of the SC and the steady-state output of the battery, without simulating long-term operating scenarios, and lacking the impact of key factors such as the life decay of the battery, thermal accumulation effect, and material aging on system reliability. In response to these limitations, the subsequent experiments will focus on long-term reliability testing, thermal behavior, stability analysis, and actual operating scenarios, providing more comprehensive data to support the engineering application of the HPS.

3.3 Comparative Case Study of The HPS and Single-Battery Systems Under The CLTC-P Operating Condition

The CLTC-P operating condition is a standardized testing procedure developed for light passenger vehicles that simulates driving characteristics on typical urban and suburban mixed roads [23] and is primarily employed to assess the vehicle's energy consumption and emission performance under typical road conditions. The CLTC-P operating condition is categorized into three distinct speed segments: low-speed, medium-speed, and high-speed, with a total duration of 1800 seconds. The low-speed segment accounts for approximately 37.4% of the overall duration, primarily simulating urban driving conditions with congestion, frequent acceleration, and deceleration. The medium-speed segment (38.5%) comprises urban expressways and ring roads, with stable driving at moderate speeds. The high-speed segment (24.1%) simulates suburban and highway conditions, evaluating power performance and energy consumption at higher speeds. The operating condition of CLTC-P is shown in Figure 15(a). To facilitate the characteristic analysis of the low-voltage HPS in this situation, when the demanded power is below 5 kW, the low-voltage HPS serves as an ancillary power supply to propel the vehicle, and the required power below 5 kW is extracted, as shown in Figure 15(b).

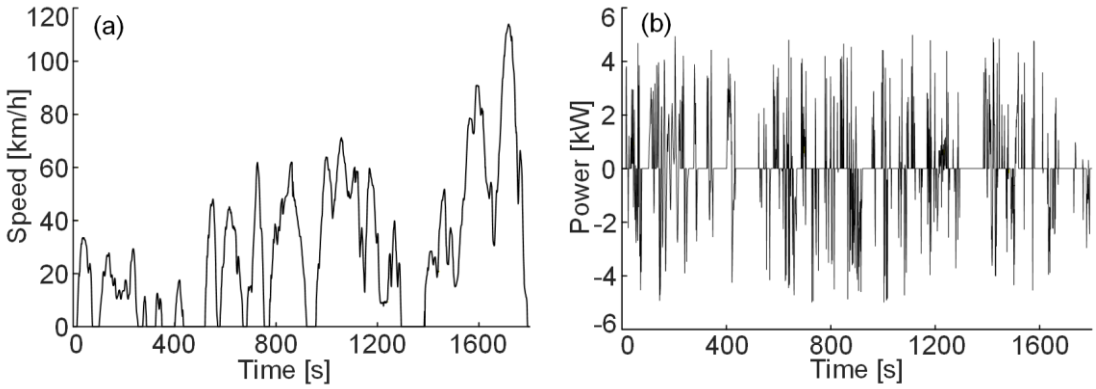

Figure 15. The CLTC-P operating condition: (a) vehicle speed, (b) required power below 5 kW

As shown in Figure 16(a), the HPS terminal voltage is approximately 14 V. The HPS current in Figure 16(b) indicates that the dynamic current is primarily supplied by the SC, with a peak of 284.48 A, while the battery provides a relatively stable current, with a maximum output of only 7.50 A. As illustrated in Figure 16(c) and Figure 16(d), the battery's SOC has consistently declined from an initial value of 80% to approximately 78.69%, with good linearity in the discharge process. The SOC of the SC decreases from 60% to about 54.89%, and although slight fluctuations are observed in its discharge curve, the overall discharge characteristics remain stable. As shown in Figure 16(e), with the Bus voltage target set to 48 V, the actual Bus voltage remains stable at an average of 48.19 V. The fluctuation amplitude is significantly lower than the design requirements, fully demonstrating the HPS's voltage stability control capability under dynamic load conditions. The load current, calculated based on operating conditions, serves as the target current value (Figure 16(f)). The actual current effectively tracks the target value, exhibiting good dynamic response. Under the CLTC-P operating condition, the HPS achieves an average efficiency of 76.2% (Figure 16(g)). Although frequent acceleration/deceleration in this operating condition results in significant energy loss, the total energy loss remains relatively low. Through comparative analysis, it can be concluded that the performance output of the HPS under this operating condition is highly consistent with that under the FTP-75 condition, thereby thoroughly verifying the stability and reliability of the proposed HPS across different operating conditions. To exhaustively assess the superiority of the HPS, two simulation scenarios based on the CLTC-P operating condition are used as comparison benchmarks. (1) A power architecture where two 14 V

batteries are directly paralleled, and then the voltage of the batteries (14 V) is increased to 48 V through a BDPC. (2) Directly using a 48 V single-battery system. The simulation results are presented in Figures 17 and 18.

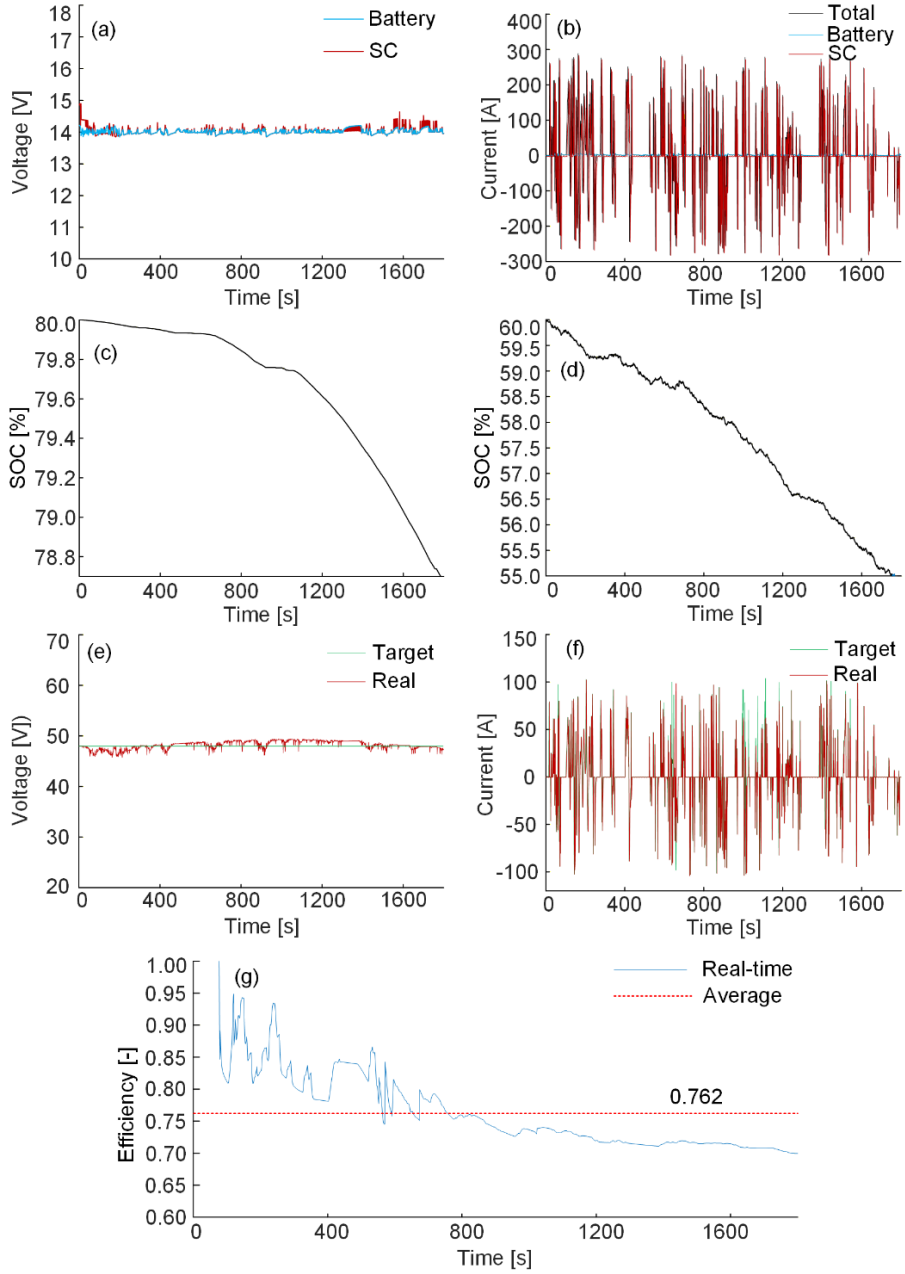

Figure 16. Simulation results under CLTC-P operating condition; (a) HPS voltage, (b) HPS current, (c) battery SOC, (d) SC SOC, (e) Bus voltage, (f) load current, (g) efficiency

In the comparison scenario (1), as shown in Figure 17(a), the battery voltage exhibits small fluctuations around the actual value of 14 V, especially during acceleration, where the fluctuations further increase. The battery current curve in Figure 17(b) shows significant fluctuations and a substantial increase in peak current. This shows that the battery needs to meet both steady-state energy output requirements and dynamic power fluctuation response, and withstand long-term high-current stress. This stress accelerates the irreversible loss of active materials, intensifies the degradation of the solid electrolyte interface (SEI) film, and ultimately shortens battery life. As depicted in Figure 17(c) and Figure 17(d), the SOC of both batteries decreases linearly from the initial value of 80% to about 74.58%, and the discharge process shows high consistency. As shown in Figure 17(e), when the Bus voltage is set with a target of 48 V, the actual Bus voltage runs stably around the average value of 47.13 V, with fluctuation amplitude controlled within ±0.5%, performing the verification of the system's capability to maintain voltage stability when subjected to dynamic load conditions. As shown in Figure 17(f), the system can track the actual current well to reach the target current when the current demand is low, exhibiting good dynamic response. However, when the demand current is high, the actual current cannot fully track the target current, indicating that the system's ability to track high-peak demand is limited. As shown in Figure 17(g), the system's average efficiency is 73.7%, which is lower than that of the HPS (76.2%).

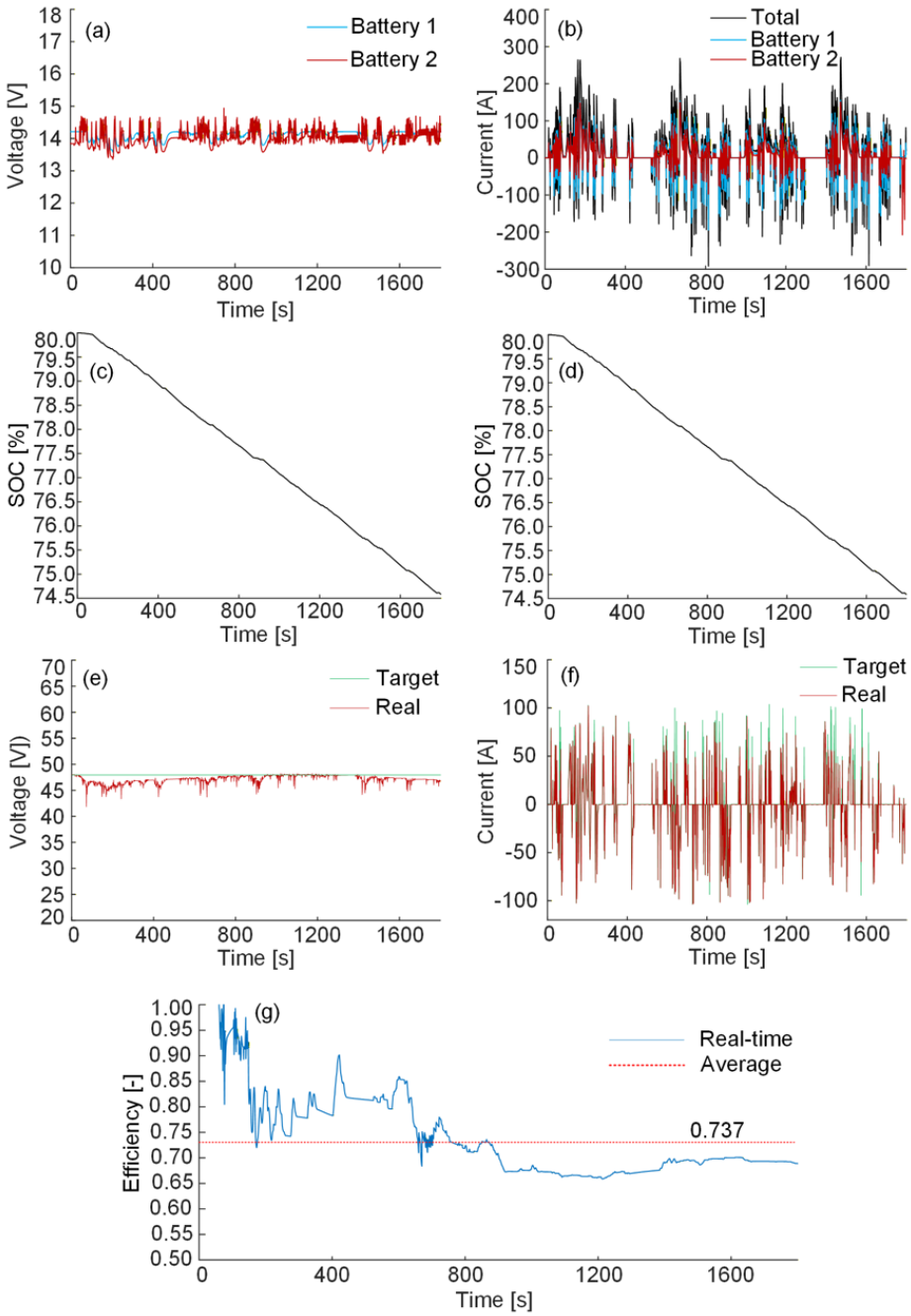

Figure 17. Simulation results with the "14 V single-battery+BDPC" system; (a) battery voltage, (b) battery current, (c) SOC of battery 1, (d) SOC of battery 2, (e) Bus voltage, (f) load current, (g) efficiency

In the comparison scenario (2), as shown in Figure 18(a), the battery voltage exhibits small fluctuations around the actual value of 48 V, especially during acceleration, where the fluctuations further increase. The current curve in Figure 18(b) shows that a single battery needs to independently bear the current demand of the complete operating condition, resulting in the battery being subjected to high current cycling stress for a long time, accelerating the loss of active materials and SEI film degradation, seriously affecting its service life. As depicted in Figure 18(c), the battery's SOC decreases from its initial value of 80% to 79.77%, and the rate of decrease shows a phased difference. For example, in the low-power demand stage, the rate of SOC decrease is slower. During the high-power demand stage, the rate of decline accelerates significantly, indicating that the system's dynamic power demand has a significant impact on SOC attenuation. As shown in Figure 18(d), the system can track the actual current well to reach the target current when the current demand is low, exhibiting good dynamic response. However, when the demand current is high, the actual current cannot fully track and reach the target, indicating that the system's ability to track instantaneous high peaks is limited. As shown in Figure 18(e), the system's average efficiency is 71.5%, which is higher than the overall system's. Compared with the 14 V "single-battery+BDPC" system and the 48 V single-battery system, the HPS offers significant advantages in dynamic response stability, system efficiency, and battery life. It can effectively avoid many problems that may occur when a single-battery system responds to dynamic power demand, thereby improving overall performance.

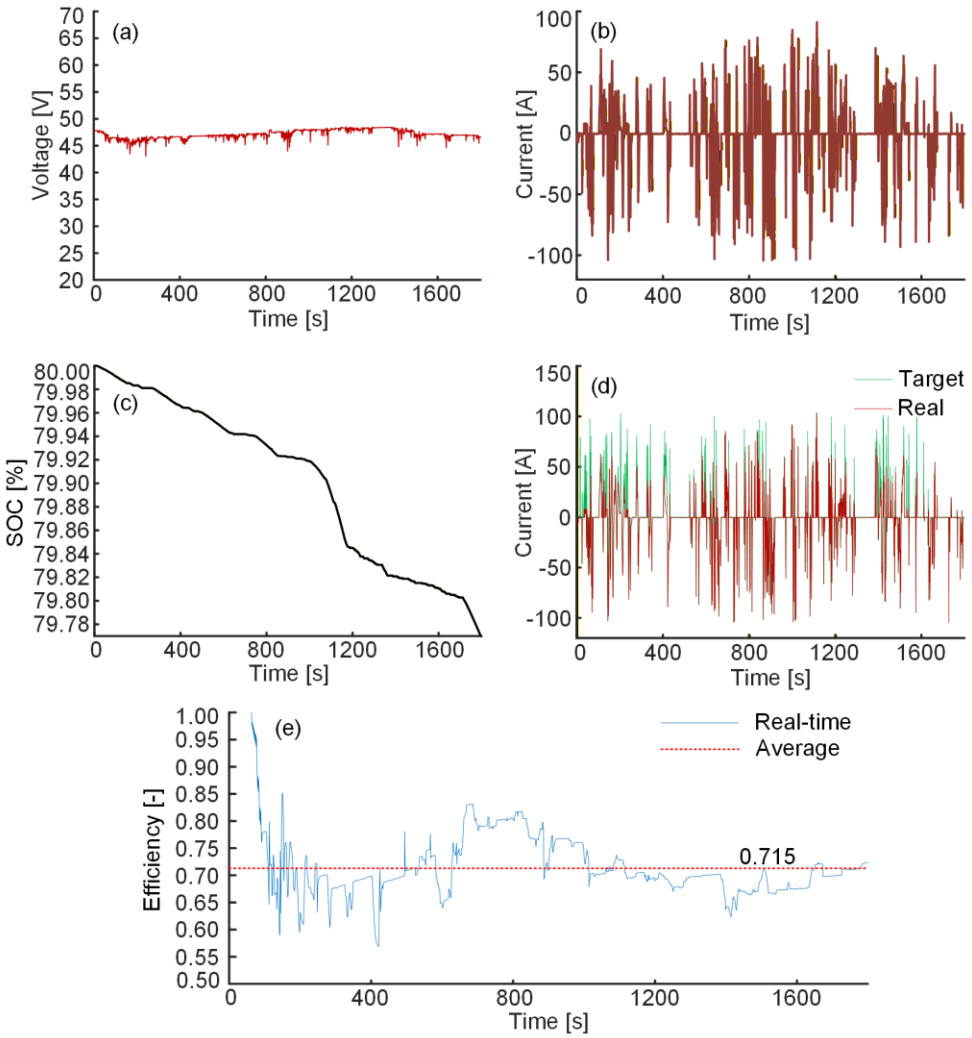

Figure 18. Simulation results with the 48 V single-battery system; (a) battery voltage, (b) battery current, (c) battery SOC, (d) load current, (e) efficiency

4. Conclusions

This study proposes a low-voltage HPS that combines a battery and SC with a BDPC. In addition to its basic function of supplying power to the electrical systems, it can also provide auxiliary power for vehicle propulsion, providing a new solution to meet the complex power requirements of vehicles. Based on a comprehensive analysis, the following key conclusions are drawn.

(i) Under the FTP-75 operating condition, the proposed HPS exhibits strong performance, with the SC peak current reaching 309.97 A, well meeting the instantaneous power demand. The battery current is limited to below 19.21 A, and the low current stress and small fluctuation amplitude are very conducive to extending the battery's service life. Furthermore, comparing the "14 V single-battery + BDPC" system and the 48 V single-battery system shows that the proposed HPS offers significant advantages in dynamic responsiveness, efficiency, and battery degradation. It effectively avoids many drawbacks of the single-battery system in responding to dynamic power demands. It provides solid support for the overall performance enhancement and functional diversification of the low-voltage power supply. This achievement not only verifies the system's scientific and rational design but also points the way for optimizing and upgrading the vehicle's low-voltage power supply.

(ii) In the variable load experiments, the dynamic performance of the HPS is verified by setting dynamic current scenarios under Bus voltages of 24 V and 30 V. The data shows that in the face of continuous step changes in load current (with a maximum amplitude of 10 A to 4 A), the SC can quickly respond and independently provide transient peak current up to 35 A, while also ensuring that the Bus voltage remains stable near the target value. Especially during high current demands (such as start-up), the SC can serve as the sole power source (with a battery output of 0 A) and successfully respond to high power demands. The rapid peak-shaving and valley-filling capabilities of the SC limit the battery current within a low-stress range, fully demonstrating the SC's core role in transient processes. By compensating the battery's power response gap in real time, the SC not only stabilizes the bus voltage but also ensures fast, accurate system output, providing high-reliability power support for the vehicle. The test results show that this collaborative working mechanism significantly improves the

dynamic performance, energy efficiency, and reliability of low-voltage power supplies under complex operating conditions of the vehicle.

(iii) The HPS has achieved complementary advantages in energy utilization through close cooperation between the two power sources, improving energy efficiency and reducing energy consumption costs. From a cost-benefit perspective, the integrated design of the HPS is not only reasonable in terms of initial investment but also provides a feasible approach to optimizing power supply costs by reducing energy consumption and maintenance costs over the long term. Therefore, the comprehensive advantages of energy complementarity and cost-effectiveness make the HPS more attractive and competitive in the market.

In summary, the HPS offers an innovative solution for vehicle power supply that combines high reliability, long lifespan, and cost-effectiveness, offering valuable technical references for optimizing the low-voltage power supply. The results not only effectively demonstrate the feasibility and superiority of the proposed solution but also reveal the SC's excellent ability to handle transient requirements in detail. This research achievement provides reliable technical support for practical engineering applications and is expected to promote the development of vehicle power supplies towards higher efficiency, reliability, and sustainability.

The future research is as follows.

(i) The configuration based on controllable architecture will be studied, aiming to achieve collaboration between the two power sources through flexible multi-mode control.

(ii) AI-driven strategies will be developed to optimize real-time power distribution weighting, balancing efficiency and complexity.

(iii) Energy control methods that consider battery states, such as SOC, state of power, and state of health, will be studied to maximize battery life and improve safety.

(iv) An aging model for long-term reliability prediction will be developed to reveal the coupling degradation mechanism between the battery and SC and to achieve accurate life prediction.

(v) Multi-objective optimization strategies will be designed to collaboratively optimize performance, durability, and efficiency across two power sources.

(vi) The testing platform will be upgraded, and a comprehensive experiment will be designed to verify the long-term stability and reliability of the HPS in real-world scenarios.

Acknowledgements

The authors would like to thank the School of Electromechanical and Automotive Engineering, Yantai University, Yantai, China, for the laboratories and other related support, and thank Zhejiang Key Laboratory of Intelligent Vehicle Comprehensive Safety and the Natural Science Foundation of Shandong Province, China

Funding

The work was supported by the foundation of Zhejiang Key Laboratory of Intelligent Vehicle Comprehensive Safety [Grant No. ZKLIVCS-202406] and the Natural Science Foundation of Shandong Province [Grant No. ZR2020ME210].

Declaration of Competing Interest

The author declares no conflicts of interest.

CRediT Authorship Contribution Statement

Caihong Yan contributed to the data curation, data analysis, resources, and validation.
Guoqing Ma was involved in supervision and funding acquisition.
Guizhou Ren contributed to review editing, conceptualization, methodology, and funding acquisition.

Availability of Data and Materials

The data supporting this study's findings are available on request from the corresponding author.

Ethics Declarations

This study did not involve human participants or animals. Ethical approval was therefore not required.

Generative Artificial Intelligence Declarations

The authors claim that artificially intelligent-assisted technologies, such as generative AI, were not used to generate content, ideas, or theories. We have just utilized AI to enhance readability and refine the language. This was used with extreme human control and oversight. The authors take full responsibility for reviewing and approving the content.

References

[1] G.W. Lin, B. Qi, C.X. Ma, "Optimization of virtual energy hub with hybrid vehicles in power-transportation networks towards a low-carbon sustainable transition: A probabilistic regret adjustment," *Sustainable Cities and Society*, vol. 120, p.106159, 2025.

[2] S.B. Shi, Y.H. Ji, L.W. Zhu, J.J. Liu, X. Gao, H. Chen, et al, "Interactive optimization of electric vehicles and park integrated energy system driven by low carbon: An incentive mechanism based on Stackelberg game," *Energy*, vol. 318, p. 134799, 2025.

[3] Z.F. Liu, Y.Y. Liu, H.J. Jia, X.L. Jin, T.H. Liu, Y. Z. Wu, "Bi-level energy co-optimization of regional integrated energy system with electric vehicle to generalized-energy conversion framework and flexible hydrogen-blended gas strategy," *Applied Energy*, vol. 390, p. 125868, 2025.
[4] P. Aruna, V. Vasan Prabhu, V. Krishnakumar, "Innovative optimization of hybrid energy storage systems for electric vehicles: Integrating FBPINN-SAO to enhance performance and efficiency," *Journal of Energy Storage*, vol. 108, p. 115021, 2025.
[5] P.K. Behera, K. Gupta, M. Pattnaik, "Hybrid energy storage unit fed motoring and regenerative braking control of electric vehicle drivetrain," *Journal of Power Sources*, vol. 626, p. 235761, 2025.
[6] R.B. Selvakumar, C. Vivekanandan, H. Sharma, V. Vekariya, R.A. Varma, V. Mohanavel, et al, "Energy management of a dual battery energy storage system for electric vehicular application," *Computers and Electrical Engineering*, vol. 115, p. 109099, 2024.
[7] K. Kalaikkanal, N. Gobinath, "A review on Lithium-ion battery failure risks and mitigation indices for electric vehicle applications," *Applied Energy*, vol. 393, p. 126139, 2025.
[8] I. Kranthikumar, C.H. Srinivas, T.V. Kiran, P. Pradeep, V. Balamurugan, "A novel hybrid approach for efficient energy management in battery and supercapacitor-based hybrid energy storage systems for electric vehicles," *Electrical Engineering*, vol. 107, pp. 1–17, 2025.
[9] Y. Zhao, F. Qin, Z. Zhang, "Robust tracking control design of hybrid battery-supercapacitor energy storage system in electric vehicles," *IEEE Transactions on Transportation Electrification*, vol. 11, no. 1, pp. 3262–3276, 2025.
[10] K. Raut, A. Shendge, J. Chaudhari, R. Lamba, N.F. Alshammari, "Modeling and simulation of photovoltaic powered battery-supercapacitor hybrid energy storage system for electric vehicles," *Journal of Energy Storage*, 82, p. 110324, 2024.
[11] W.R. Liu, P.F. Yao, Y. Wu, L.J. Duan, H. Li, J. Peng, "Imitation reinforcement learning energy management for electric vehicles with hybrid energy storage system," *Applied Energy*, vol. 378, p. 124832, 2025.
[12] B.X. Lin, G.Z. Ren, "Power distribution methods of ultra-capacitor/battery hybrid power source for vehicular applications," *International Journal of Vehicle Design*, vol. 93, no 1-2, pp. 87–119, 2023.
[13] X. Li, M.H. Li, M. Habibi, N. Najaafi,d H. Safarpour, "Optimization of hybrid energy management system based on high-energy solid-state lithium batteries and reversible fuel cells," *Energy*, vol. 283, p. 128454, 2023.
[14] R. Kannan, C. Kalaivani, G. Devadasu, "Energy management in plug-in hybrid electric vehicles with hybrid energy storage system using hybrid approach," *Energy Technology*, vol. 10, no. 10, p. 2200355, 2022.
[15] O. A. Alkawak, J. R. R. Kumar, S. S. Daniel, C.V. K. Reddy, "Hybrid method based energy management of electric vehicles using battery-supercapacitor energy storage," *Journal of Energy Storage*, vol. 77, p. 109835, 2024.
[16] H. Chen, R. Xiong, C. Lin, and W.X. Shen, "Model Predictive control based real-time energy management for hybrid energy storage system," *CSEE Journal of Power and Energy Systems*, vol. 7, no. 4, pp. 862–874, 2021.
[17] N.D. Nguyen, C.W. Yoon, Y.I. Lee, "A standalone energy management system of battery/supercapacitor hybrid energy storage system for electric vehicles using model predictive control," *IEEE Transactions on Industrial Electronics*, vol. 70, no. 5, pp. 5104–5114, 2023.
[18] G.Z. Ren, J.Z. Wang, Y.Y. Li, G.F. Zhang, "Power distribution optimization of a fully active hybrid energy storage system configuration for vehicular applications," *Journal of Industrial Information Integration*, vol. 33, p. 100459, 2023.
[19] M. Robayo, M. Mueller, S. Sharkh, M. Abusara, "Assessment of supercapacitor performance in a hybrid energy storage system with an EMS based on the discrete wavelet transform," *Journal of Energy Storage*, vol. 57, p. 106200, 2023.
[20] G.Z. Ren, Y.Y. Li, J. X. Zhang, Y.P. Duan, Y.Q. Si, C.H. Yan, "Power distribution optimization for hybrid power source integrated with battery and super-capacitor considering vehicle energy consumption," *Energy Conversion and Management*, vol. 306, p. 118298, 2024.
[21] G.Z. Ren, H.R. Wang, C.L. Chen, J.Z. Wang, "An energy conservation and environmental improvement solution-ultra-capacitor/battery hybrid power source for vehicular applications," *Sustainable Energy Technologies and Assessments*, vol. 44, p. 100998, 2021.
[22] MathWorks, "Generic battery model," *MathWorks Documentation*, 2024. [Online]. Available: https://ww2.mathworks.cn/help/sps/powersys/ref/battery.html.
[23] D. Tan, J.W. Tan, M. Liu, H.L. Xu, Y.S. Ge, "A combined vehicle-specific power and laboratory emissions approach to real driving CO2 emission estimation for light-duty vehicle," *Sustainable Energy Technologies and Assessments*, vol. 75, p. 104265, 2025.